

Stereochemical analysis of deuterated alkyl chains by charge-remote fragmentations of protonated parent ions

Kangling Zhang^a, Stephane Bouchonnet^b, Scott V. Serafin^a, Thomas Hellman Morton^{a,*}

^a Department of Chemistry, University of California, Riverside, CA 92521-0403, USA

^b DCMR, Ecole Polytechnique, 91128 Palaiseau, France

Received 20 November 2002; accepted 6 January 2003

Dedicated to Rob Dunbar on the occasion of his 60th birthday.

Abstract

MH⁺ ions from *sec*-alkyl *m*-dimethylamino ethers have been studied by MS/MS using chemical ionization (CI) and electrospray ionization (ESI). Collisionally activated dissociation (CAD) of MH⁺ from the vicinally perdeuterated 3-hexyl ether, CH₃CD₂CHOArCD₂CH₂CH₃, shows that alkene expulsion is >96% regioselective, yielding *m/z* 139 and *m/z* 124 fragment ions. The fact that alkene elimination is not 100% regioselective (but gives about 3% *m/z* 138) is attributed to a small amount of ion–neutral complex formation. CAD of MH⁺ ions from vicinally monodeuterated ethers (the 3-hexyl-4-*d*₁ ether (**1**) and the *sec*-butyl-3-*d*₁ ether (**2**)) demonstrates that the *erythro* and *threo* diastereomers give significantly different *m/z* 139:*m/z* 138 fragment ion intensity ratios. These intensity ratios are sufficiently reproducible that they can be used to quantitate the proportions of *erythro* and *threo* in mixtures. DFT calculations show substantial differences between the 4-center transition states for charge-remote elimination vs. alkene elimination from a neutral precursor.

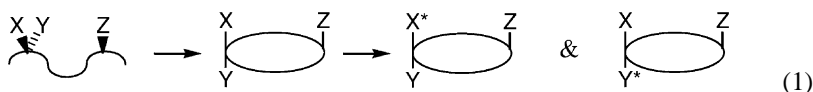
© 2003 Published by Elsevier Science B.V.

Keywords: Vicinal elimination; Density functional theory; 4-Center transition state; Dissociative resonance structures; Zwitterion; Keto–enol tautomerization

1. Introduction

MS/MS techniques have greatly expanded the scope of mass spectrometry as an analytical tool. One useful application has been used to determine the configurations of molecules that are chiral by virtue of isotopic substitution. The method introduced nearly 25 years ago involves converting an acyclic product to a cyclic

derivative that allows stereochemical positions to be differentiated chemically, and then to perform MS/MS analysis to discern the location of a given isotopic substituent on the ring [1]. Eq. (1) depicts this strategy schematically, where X and Y stand for different isotopes of the same element, Z a substituent in a stereochemically defined reference position, and X* and Y* chemical modifications of the original isotopic atoms.



* Corresponding author. Tel.: +1-909-787-4725;

fax: +1-909-787-4713.

E-mail address: morton@citrus.vcr.edu (T.H. Morton).

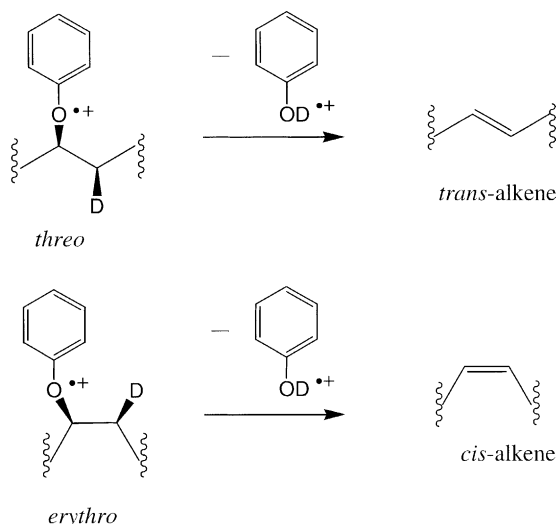
In the first step, the acyclic molecule of interest is converted to the cyclic derivative in the middle. Then one or the other of the isotopic atoms is covalently modified to give a mixture of separable isomers, drawn to the right. Once the isomers have been separated and identified, MS/MS techniques can be used to tell which isotope is retained when the asterisked group is lost. The original application addressed the problem of identifying the configuration of a phosphate group containing all three stable oxygen isotopes. Two stages of mass spectrometry were required after purification of one of the cyclic derivatives, because it was necessary to differentiate the cyclized parent ions containing ^{16}O and ^{17}O from the ones containing ^{16}O and ^{18}O or ^{17}O and ^{18}O [1].

Despite the elegance of this mass spectrometric technique, it is complicated by the necessity of a separation step prior to mass spectrometric analysis. Moreover, although the predominant configuration can be assigned, the relative abundance of the minor component cannot be quantified with high precision in a mixture of isomers. In approaching the issue of quantitation, we have been examining the problem of measuring the ratios of stereoisomers that differ by the placement of a deuterium relative to a hydrogen. In these experiments, we have been guided by the observation that ions derived from alkyl aryl ethers expel alkene as the predominant mass spectrometric fragmentation [2]. There turns out to be a dramatic change in the unimolecular decomposition mechanism in going from a primary to a secondary alkyl group. Specifically, alkene expulsion from acyclic *sec*-alkyl aryl ethers proceeds via cyclic transition states. This obviates the need to prepare (and purify) cyclic derivatives prior to mass spectrometric analysis.

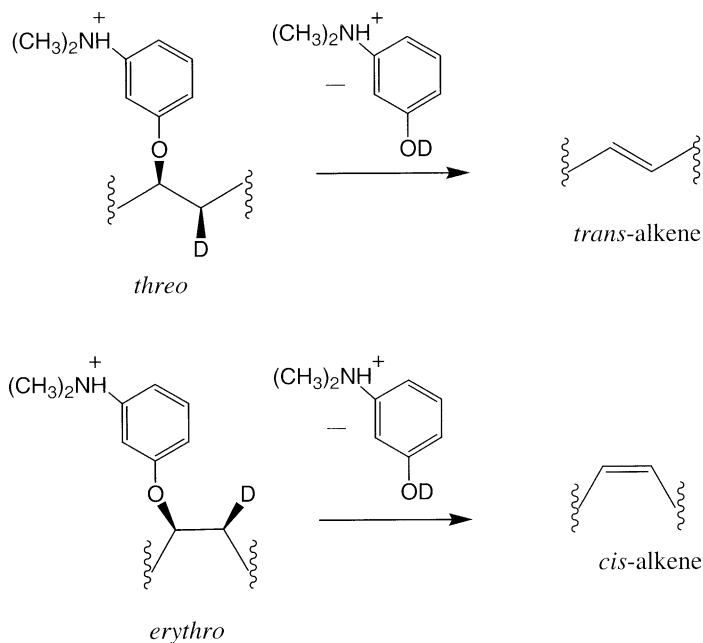
Trapped ion photodissociation experiments performed in the Dunbar laboratory demonstrated that the barrier for propene expulsion from ionized isopropyl phenyl ether is significantly lower than from ionized *n*-propyl phenyl ether [3] and imply that the former reaction operates via a 4-center cyclic transition state. A deuterium labeling experiment showed that *sec*-alkyl aryl ether ions prefer to eliminate *trans* rather than *cis* alkenes via this pathway [4], which has

led to a mass spectrometric method of distinguishing secondary alcohols (by means of their phenyl ethers) that are diastereomeric by virtue of deuterium substitution on an adjacent carbon [5]. We have shown that this technique is capable of measuring the proportions of two diastereomers in a mixture [6] and herein describe improvements in this method using charge-remote fragmentations of protonated parent ions.

Scheme 1 represents this technique for the molecular ions of *sec*-alkyl phenyl ethers that have a single deuterium on an adjacent methylene. The two diastereomers (conventionally designated *threo* and *erythro*) yield ionized phenol ($\text{PhOH}^{\bullet+}$, m/z 94) as the base peak in the source mass spectrum, as well as in the MIKE and collisionally activated dissociation (CAD) spectra of the molecular ions. Lower abundances of the deuterated ion ($\text{PhOD}^{\bullet+}$, m/z 95) occur, with the m/z 95: m/z 94 intensity ratio depending on the relative stereochemistry of the phenoxy and deuterium. As Scheme 1 represents, *syn*-elimination of $\text{PhOD}^{\bullet+}$ from the *threo* isomer expels a *trans* alkene, while *syn*-elimination from the *erythro* expels a *cis* alkene. Because *trans* is thermodynamically favored over *cis*, a higher proportion of m/z 95 is observed in the case of *threo* deuteration from every ionized *sec*-alkyl phenyl ether, $\text{ROPh}^{\bullet+}$, from R = butyl to R = octyl [5].



Scheme 1.



Scheme 2.

In endeavoring to refine the quantitative analysis of mixtures of diastereomeric alcohols, we consider four variables: (1) the derivatization of the alcohol as an aryl ether; (2) the method of ionization of the aryl ether; (3) the means by which the first stage of mass selection is accomplished prior to CAD; and (4) the nature of the CAD itself. This paper looks at the *meta*-dimethylaminophenyl ethers of deuterated 2-butanol and 3-hexanol and concludes that CAD of the protonated parent ions, illustrated in Scheme 2, yield results comparable to the ionized phenyl ethers in Scheme 1, but with an improvement in precision.

The alkene expulsion in Scheme 2 may be viewed as a charge-remote fragmentation. In other words, the site of reaction is removed from the position where the electric charge is localized. Among the questions raised are the following. Does the mechanism for Scheme 2 differ from that of Scheme 1? Does the presence of a remote charge make a difference in comparison with elimination from a neutral molecule? Do the specificities of Schemes 1 and 2 differ?

With regard to the mechanism of Scheme 1, FT-ICR experiments have shown that the deuterium from the alkyl chain is deposited onto the phenoxy oxygen [6], ruling out transfer to the benzene ring. As Section 4 will demonstrate, DFT calculations predict that the same pathway must operate for Scheme 2. A computational comparison of the charge-remote and the neutral fragmentations shows significant differences in barrier heights, which are, in turn, much higher than the experimental activation energies for ionized phenyl ethers. Nevertheless, the specificities for charge-remote and radical cation fragmentations are nearly the same.

2. Experimental section

m-Dimethylaminophenyl ethers were synthesized via two approaches and introduced into the instruments without further purification. The 3-hexyl-2,2,4,4-*d*₄ ether, 1- β,β' -*d*₄, was prepared via NaOD-catalyzed repetitive exchange of 3-hexanone with D₂O, followed by reduction with lithium aluminum hydride,

conversion of the d_4 -alcohol to the corresponding tosylate, and nucleophilic displacement by sodium m -dimethylaminophenoxide in THF. Monodeuterated m -dimethylaminophenyl ethers e -1- β - d_1 , t -1- β - d_1 , e -2- β - d_1 , and t -2- β - d_1 were prepared by attack of the corresponding epoxides (*cis*-3,4-epoxyhexane, *trans*-3,4-epoxyhexane, *cis*-2,3-epoxybutane, and *trans*-2,3-epoxybutane, respectively) by sodium m -dimethylaminophenoxide in THF, followed by conversion to the corresponding tosylates and reduction with lithium aluminum deuteride, in a fashion analogous to the preparations of deuterated phenoxyalkanes [5]. Diastereomeric purities (based on the stated isomeric purities of the commercially available starting materials: *cis*-3-hexene, *trans*-3-hexene, and the epoxybutanes) were >98%. The latter method of synthesis yielded material containing small amounts of alkenyl m -dimethylaminophenyl ethers (from elimination of tosic acid in the final step), while both methods gave a few percent of ring-alkylated m -dimethylaminophenols (via nucleophilic attack by a m -dimethylaminophenoxide carbon rather than by oxygen). These impurities were separated from the major products by means of their chromatographic introduction into the MS/MS instruments.

Electron ionization (EI) 70 eV spectra were obtained on a ZAB 2F two-sector (B–E) mass spectrometer via direct introduction through a liquid sample inlet. Mass-analyzed ion kinetic energy (MIKE) and CAD spectra were recorded (with helium used as the collision gas for CAD experiments) and digitized, and overlapping peaks were resolved using Gaussian fits using IGOR Pro software version 4.0 (WaveMetrics, Inc., Lake Oswego, OR). GC/CI experiments were performed on a Saturn 2000 GC/ion trap instrument by injecting acetonitrile solutions of m -dimethylaminophenyl ethers of deuterated 2-butanol and 3-hexanol onto a 30 m \times 0.25 mm CP-Sil 8 CP WCOT fused silica capillary column, with chemical ionization (CI) using added acetonitrile as reagent gas. MH^+ ions were isolated using a 5 ms isolation time. CAD was performed in resonant mode using 0.55–0.6 V excitation amplitude, which gave virtually complete dissociation of the MH^+ parent ions. Other excitation

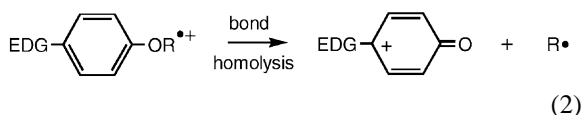
amplitudes were examined, which gave comparable m/z 138: m/z 139 intensity ratios, but the values chosen gave the best reproducibility: lower voltages gave less abundant fragmentation (and significant levels of undissociated MH^+), while higher voltages led to further fragmentation (principally via loss of methyl in addition to alkene expulsion).

LC/Q-ToF experiments were performed using sample introduction via a capillary HPLC (Agilent 1100) using an Agilent 0.5 mm \times 150 mm ZORBAX SB-C18 column (5 μ m particle diameter, 80 Å pore size), with mobile phases A (0.1% formic acid in water) and B (0.1% formic acid in acetonitrile) used with a linear gradient of 45–90% of mobile phase B over 60 min followed by 90% of mobile phase B for 5 min at a flow rate of 6 μ L min⁻¹. The flow was directly introduced into the electrospray source of a Q-ToF mass spectrometer (Q-ToF Ultima-Global, Micromass, UK). Samples of 1 μ L with a concentration of approximately 1 μ g mL⁻¹ in 60% methanol were injected for each run. Q-ToF experiments were performed at a capillary voltage of 3.0 kV and a cone voltage of 77 V. The source block and desolvation gas (Nitrogen) temperatures were 90 and 120 °C, respectively. CAD experiments were performed in a hexapole collision cell using argon (4 psi) as the collision gas. Collision energies were varied from 8 to 18 eV and were optimized at nominal 12 eV (measured voltage 11.4 eV). The quadrupole mass filter before the ToF analyzer was set with LM and HM resolution settings of 15.5 (arbitrary units), which is approximately equivalent to a 0.5-Da mass window for transmission of precursor ions when a low ion energy of 0.9 V is chosen. For measurement of ion intensity ratios, the Q-ToF mass spectrometer was operated in a constant CAD mode for the entire LC run, with the mass spectrometer set to acquire CAD spectra on a single precursor ion m/z value. Ion intensity ratios from CAD of MH^+ ions from e -1- β - d_1 , t -1- β - d_1 , and diastereomer mixtures are based on three to five independent trials comprising a total of 9–16 measurements, which were averaged. Experimental data points were interpolated by fitting to a cubic polynomial function in order to construct calibration curves.

DFT computations were performed at the B3LYP/6-31G** level using GAUSSIAN98, with zero point energies and entropies based on unscaled normal mode frequencies calculated at that level. Basis set superposition error was estimated using counterpoise. The imaginary frequencies for transition states ($444i$ and $1525i\text{ cm}^{-1}$ for Figs. 3 and 4, respectively) were visualized using GaussView2.1 and found to correspond to the expected reaction coordinates.

3. Results

The *m*-dimethylaminophenyl ethers were chosen for two reasons: the commercial availability of the corresponding phenol and the lack of conjugative connection between the nitrogen and the oxygen. In previous studies of phenyl ethers substituted with an electron-donating substituent (EDG) in the *para* position, a tendency for their radical cations to undergo simple bond homolysis was noted [7], as Eq. (2) depicts. Since we wished to avoid that competing fragmentation, the *meta* isomer was preferred over the *ortho* or *para* substitution.



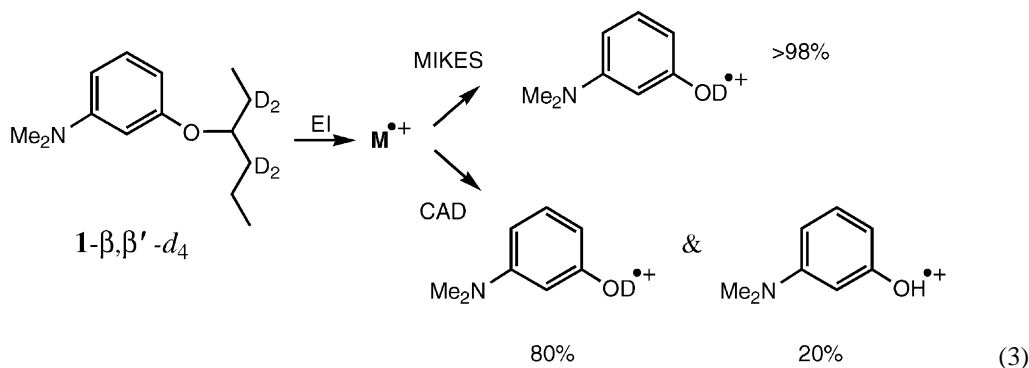
3.1. Regioselectivity

Our first objective was to examine the regioselectivity of alkene elimination. To that end we examined

the β,β' -perdeuterated 3-hexyl- d_4 ether, $1-\beta,\beta'-d_4$, drawn in Eq. (3). Previous studies have shown that ionized *sec*-alkyl phenyl ethers decompose predominantly via *syn*-elimination, but that a small proportion forms the same decomposition products via intermediate ion–neutral complexes (which lead to rearrangement and hydrogen shifts from other carbons besides those in the β -position) [8]. While the metastable ion decompositions of ionized $1-\beta,\beta'-d_4$ showed virtually complete regioselectivity, as Eq. (3) summarizes, its CAD fragmentation pattern in the same instrument showed a significant level of hydrogen transfer from other positions, signaling that competition from ion–neutral complex-mediated pathways cannot be neglected.

Further experiments have, therefore, focused on the protonated parent ions of *m*-dimethylaminophenyl ethers. CI of $1-\beta,\beta'-d_4$ with acetonitrile in the GC/QIT gives an $M^{\bullet+}$: MH^+ (m/z 225: m/z 226) intensity ratio of approximately one-third. The best isolation that we were able to achieve through selective ion ejection using standard settings for the isolation time still had an m/z 225 intensity nearly 6% that of m/z 226.

CAD of chemically ionized $1-\beta,\beta'-d_4$, as summarized in Table 1, shows that elimination of hexane does not occur with 100% regioselectivity. Exclusive *syn*-elimination would yield only m/z 139, but a small amount of m/z 138 is observed, as Eq. (4) summarizes. The proportion of m/z 138 is greater than can be accounted for by fragmentation of the m/z 225 parent ion that accompanies m/z 226 in the CI/ion trap experiment. One possible hypothesis is



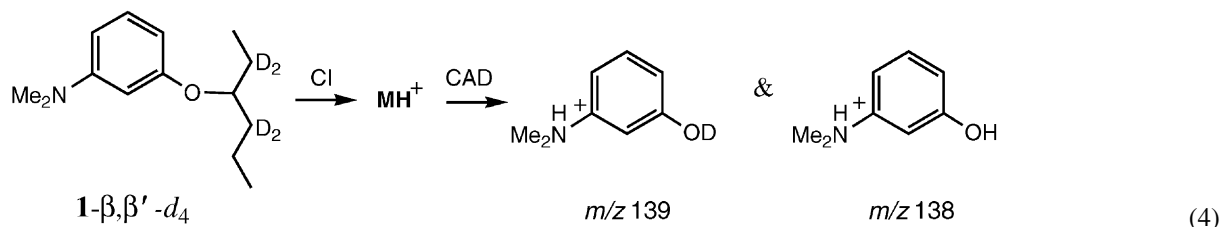


Table 1

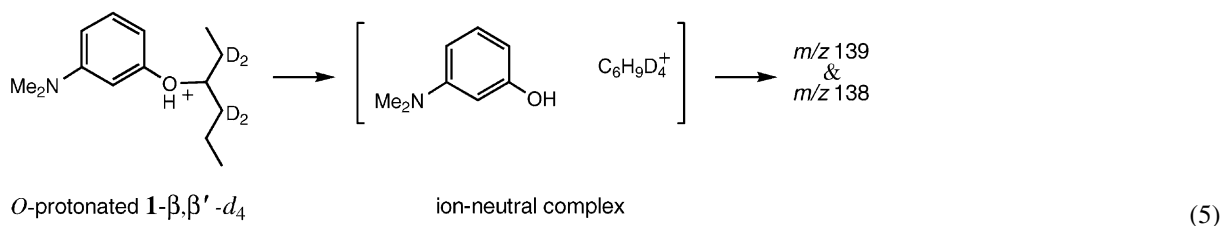
Relative intensities of parent and fragment ions from resonant excitation (nominal 0.6 V unless otherwise specified) CAD of MH^+ ions in the ion trap (from acetonitrile CI of the leading edge of the GC peak)

	m/z 123	m/z 124	m/z 138	m/z 139	$MH^+ - CH_3$	MH^+
1-β,β'-d₄ (0.4 V)	<0.01	0.085	0.145	1	0.03	0.22
1-β,β'-d₄ (0.6 V)	0.07	0.255	0.195	1	0.02	0.015
<i>e</i> -2-β- <i>d</i> ₁	0.155	0.045	1	0.225	0.02	0.035
<i>t</i> -2-β- <i>d</i> ₁	0.15	0.065	1	0.265	0.015	0.05

that EI on acetonitrile produces ions that are acidic enough to protonate the parent neutral on oxygen, and that the *O*-protonated MH^+ ion can decompose via ion–neutral complexes, as Eq. (5) depicts. That would no longer be a charge-remote fragmentation, and the isotopic label might well be expected to scramble within the $C_6H_9D_4^+$ cation inside the complex, before it undergoes a Brønsted acid–base reaction with its neutral partner.

To test whether Eq. (5) fully accounts for the production of m/z 138 from the protonated parent ion, electrospray ionization (ESI) of **1-β,β'-d₄** was examined. As Fig. 1 summarizes, dissociation of the parent ion is not complete under the conditions used (unlike the GC/ion trap experiments, where dissociation of MH^+ was virtually complete). As the upper curve in Fig. 1 shows, the intensity of the MH^+ ion was greater than that of the most intense decomposition fragment, m/z 139, at all voltages studied.

There can be little doubt that, in solution, only the *N*-protonated ion forms, and it seems reasonable to assume that no *O*-protonated ion is created when a solution is electrosprayed into the Q-ToF. Nevertheless, a small amount of m/z 138 still persists in the CAD spectrum. Fig. 1 shows that this proportion ($3.3 \pm 0.8\%$ of m/z 139 intensity) does not vary monotonically with collision energy. As collision energy increases, however, the amount of subsequent loss of methyl radical (which produces m/z 124) increases markedly, possibly as the result of multiple collisions. A quadratic fit of the m/z 138: m/z 139 intensity ratio as a function of voltage shows a minimum at around 12 eV nominal collision energy. Q-ToF studies of stereoselectivity were, therefore, performed at that voltage, which also represented a suitable compromise between increasing the amount of MH^+ decomposition, on the one hand, and minimizing the amount of additional methyl loss, on the other.



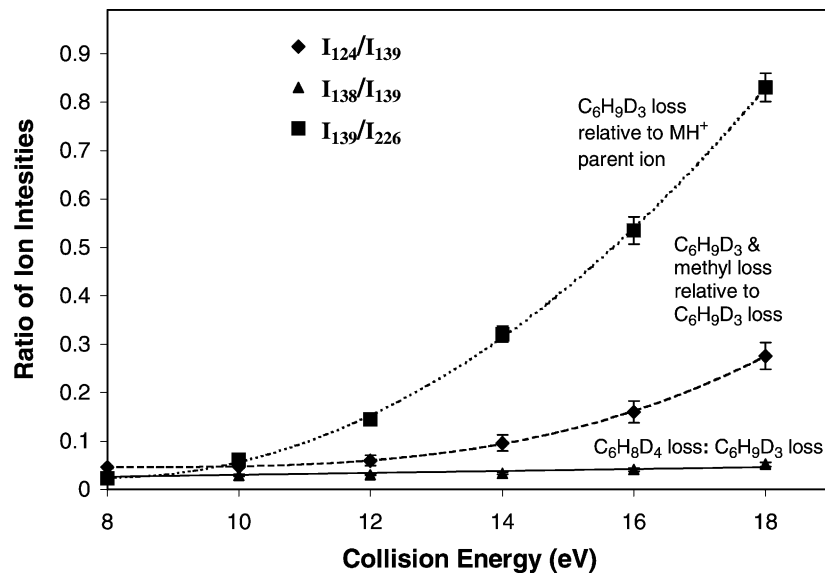


Fig. 1. Results of CAD on m/z 226 (MH^+) from $1-\beta,\beta'$ - d_4 as a function of nominal collision energy, comparing vicinal alkene elimination (m/z 139) with other ion intensities. Error bars represent standard errors of the means.

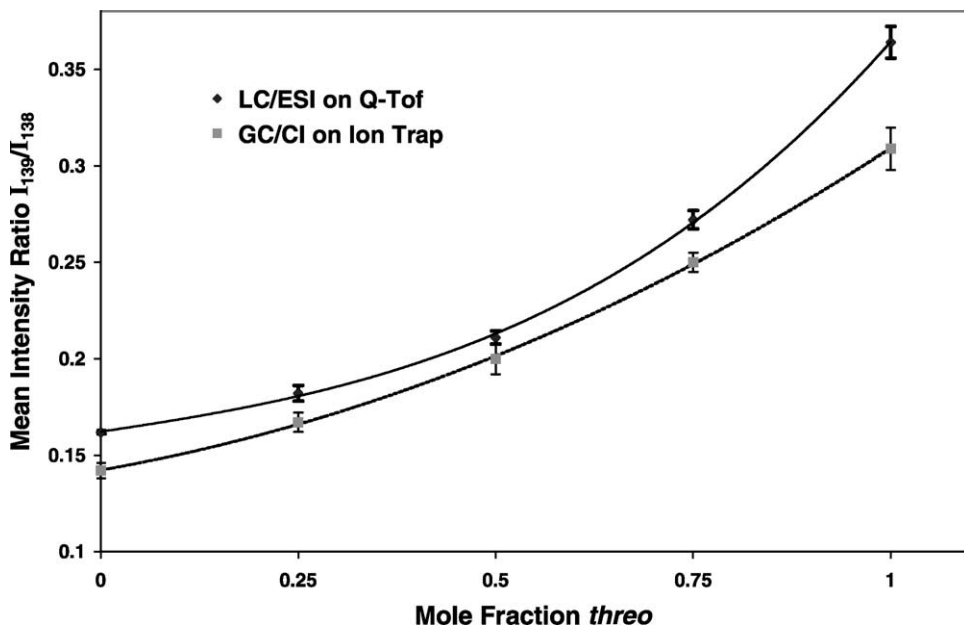


Fig. 2. Calibration curves showing ion intensity ratios (m/z 138: m/z 139) for various mixtures of diastereomeric m -dimethylaminophenyl 3-hexyl-4- d_1 ethers. The lower curve fits the data for GC/ion trap experiments using CI. The upper curve fits the data for LC/Q-ToF experiments using ESI. Error bars represent standard errors of the means.

GC/ion trap study, as the upper curve in Fig. 2 summarizes. In order to confirm the accuracy of observed ratios, the CAD spectra of the MH^+ ions of *e*- and *t*-**1**- β -*d*₁ were also examined using direct introduction into the electrospray source of a triple quadrupole MS/MS [10] and found (within experimental error) to give the same *m/z* 139:*m/z* 138 ratios as observed in the ion trap and Q-Tof.

4. Discussion

Two mechanisms compete in the expulsion of alkenes from alkyl phenyl ether ions: concerted *syn*-elimination via 4-center transition states [9] vs. a stepwise pathway via ion–neutral complexes [7]. The former mechanism is regioselective and stereospecific, while the latter is not. The present work has sought to minimize the contribution from ion–neutral complexes in order to optimize the observable stereoselectivity. As Eq. (3) indicates, the lack of complete regioselectivity in the CAD of $M^{\bullet+}$ ions from *m*-dimethylaminophenyl ethers implies a substantial contribution from complex-mediated pathways. To abolish that component, we turn to a charge-remote fragmentation, the CAD of protonated parent ions. Surprisingly, regioselectivity has not been found to be 100% complete, even when the MH^+ ions were generated by ESI. The degree of regioselectivity is nevertheless very high (>96%). DFT calculations described below compare the 4-center transition state for the charge-remote fragmentation with other reactions.

4.1. The transition state for charge-remote fragmentation

The $M^{\bullet+}$ ions from *m*-dimethylaminophenyl ethers show less regioselectivity in their CAD than do the $M^{\bullet+}$ ions from phenyl ethers [5], but the MH^+ ions exhibit greater regioselectivity. The experimental data support the following inferences: (1) transfer of β -hydrogen is highly favored for MH^+ , and (2) the degree of stereoselectivity is great enough that the diastereomer content of mixtures can be quantitated

using mass spectrometry. Fig. 3 summarizes the results of DFT calculations on *syn*-elimination from *N*-protonated **2** via a 4-center transition state.

The elimination of alkene from *N*-protonated *m*-dimethylaminophenyl ethers is a charge-remote fragmentation. As a consequence, both the net endothermicity and the activation barrier are higher than for $M^{\bullet+}$ ions, in which the electric charge is delocalized. The endothermicity of propene expulsion from *i*PrOPh $^{\bullet+}$ is $101 \pm 4 \text{ kJ mol}^{-1}$ [3], approximately 20 kJ mol^{-1} lower than the zero Kelvin endothermicity calculated for *trans*-2-butene elimination from *N*-protonated **2**, summarized in Fig. 3. Likewise, the experimental activation barrier for propene expulsion from *i*PrOPh $^{\bullet+}$ is $<128 \text{ kJ mol}^{-1}$, as compared with the DFT barrier for the charge-remote elimination in Fig. 3, $\Delta H^\ddagger = 186 \text{ kJ mol}^{-1}$.

The DFT-calculated transition state for the charge-remote elimination differs from the reactant geometry in several ways. The carbon to which oxygen was initially attached becomes planar in the transition state. The carbon from which hydrogen is migrating has also extensively flattened out (the sum of its three bond angles is 351° , as compared to 331° in the MH^+ parent ion, *N*-protonated **2**). The four atoms in the cyclic transition state are coplanar, and the bond lengths and bond angles are summarized in Fig. 3. The transition state, however, is loose, as indicated by the positive activation entropy. Other differences between reactant and transition states will be discussed below in comparing charge-remote elimination with elimination from neutral **2**.

After passing through the transition state, the ion and neutral retain some attraction for one another. The resulting energy minimum should not be confused with an ion–neutral complex. In the case of *trans*-2-butene and *N*-protonated *m*-dimethylaminophenol, the local minimum containing these two partners corresponds to a hydrogen-bonded complex, but the neutral does not necessarily dwell in the vicinity of the ion long enough for the partners to stay together an appreciable length of time.

The following computational evidence supports the conclusion that the minimized geometry corresponding

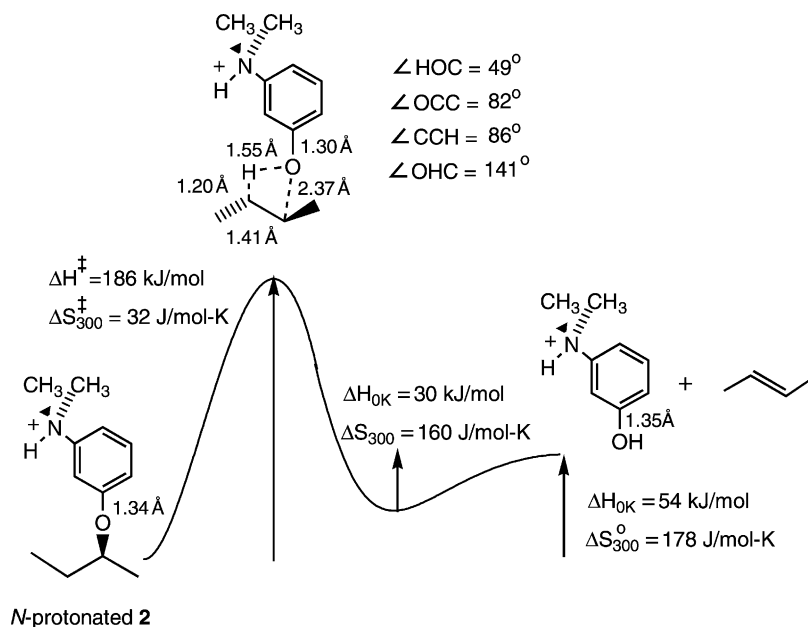


Fig. 3. Schematic DFT energy surface for expulsion of *trans*-2-butene from *N*-protonated **2**, showing the reactant ion, the 4-center transition state (with activation parameters), the hydrogen-bonded complex of the elimination products (along with corresponding reverse activation parameters), and the final products (with thermochemistry), as well as relevant geometrical features.

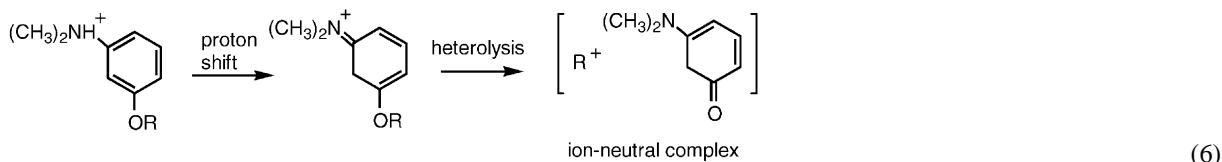
to the local minimum in Fig. 3 is hydrogen-bonded: (1) the NH stretch is shifted to lower frequency by 270 cm^{-1} relative to that of *N*-protonated *m*-aminophenol; (2) the N–H bondlength increases by 0.015 \AA and the N–H proton forms an isosceles triangle with the two sp^2 carbons of *trans*-2-butene (each leg 2.41 \AA); (3) the lowest frequency normal mode that displaces rigid 2-butene to distort this triangle corresponds to a 62 cm^{-1} vibration, a frequency much higher than would be expected if only ion-induced dipole forces held the partners together; and (4) the net zero point energy of this local minimum lies between that of the 4-center transition state and that of *N*-protonated **2** (12 kJ mol^{-1} higher than the former and 10 kJ mol^{-1} lower than the latter).

4.2. Contribution from ion–neutral complexes

It is somewhat surprising that the alkene expulsion from *N*-protonated ethers is not 100% regioselective. While elimination from the β, β' - d_4 radical ion

(Eq. (3)) or the *O*-protonated tautomer might plausibly proceed via ion–neutral complexes as a competing pathway to yield m/z 138 as well as m/z 139, it is not so easy to see how the *N*-protonated parent ion might do so. Nevertheless, an intermediate ion–neutral complex represents virtually the only way that an alkene might be expelled via transfer of hydrogen from a site other than one of the β -positions.

Three hypotheses present themselves. The first assumes that the hydrogen-bonded complex represented by the local energy minimum in Fig. 3 might live long enough to exchange D^+ for H^+ . Such a transposition would, however, require a sequence of improbable steps: transfer of H^+ from nitrogen to one of the carbons of the alkene ($>70 \text{ kJ mol}^{-1}$ endothermic, based on the proton affinity differences between aniline and C_6H_{12} [11]), return of H^+ to the oxygen, transfer of D^+ to the alkene, and return of H^+ to the nitrogen. Since the hydrogen-bonded complex is bound by only 20 kJ mol^{-1} , the first proton transfer step would be expected to be very much slower than dissociation to the



final products. Thus, a post-elimination exchange can be ruled out.

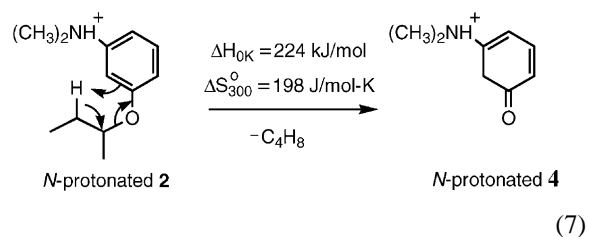
An alternative hypothesis supposes that a minor pathway for elimination involves simple cleavage to create a complex containing a zwitterionic tautomer of *m*-dimethylaminophenol (**3**). DFT calculations place the zero Kelvin heat of formation of zwitterion **3** at least 175 kJ mol⁻¹ higher than that of the phenol itself. If a [hexyl cation **3**] complex were forming, one would expect its energy to be so high that the proportion of *m/z* 138 from **1**- β,β' -*d*₄ ought to increase with collision energy. The experimental data summarized in Fig. 1 indicate that the *m/z* 138:*m/z* 139 ratio does not vary significantly with collision energy, at the same time as the proportion of subsequent methyl loss rises substantially. Therefore, the formation of [hexyl cation **3**] complexes is also excluded.

The third hypothesis suggests that a unimolecular proton shift takes place a small fraction of the time, whereby a [hexyl cation **4**] complex forms, as Eq. (6) illustrates. Cyclohexadienone (**4**) is a keto tautomer of the phenol, whose zero Kelvin heat of formation lies 44 kJ mol⁻¹ higher in energy. A proton transfer from nitrogen to the ring via a cyclic transition state would have to take place in order for such a complex to form. Such a transition state (either via a 3-membered ring to make the *ipso*-protonated ion first or via a 4-membered ring to make the more stable precursor of the ion–neutral complex directly) appears possible and seems the most plausible of the three options.

4.3. Other elimination mechanisms

Given the likelihood that complexes containing **4** form in competition with regioselective elimination, the question arises as to whether the charge-remote elimination of alkenes might operate via a 6-center

transition state as Eq. (7) depicts. The ionic product from this mechanism would have the structure of an *N*-protonated **4**. Thermochemistry argues against competition from Eq. (7). The nitrogen of **4** is not basic, since it is conjugated with the carbonyl group via the two intervening double bonds. (Hence, the C=O bond of **4** is calculated to be longer than ordinary unsaturated carbonyl groups, which typically have bondlengths of 1.21 Å at this level of computation.) Compound **4** behaves like an amide (it is called a “vinylogous amide”). DFT calculations place the heat of formation of *N*-protonated **4** 101 kJ mol⁻¹ higher than that of *N*-protonated *m*-dimethylaminophenol. The thermodynamic barrier to the expulsion of *trans*-2-butene in Eq. (7) exceeds the barrier height for the 4-center elimination represented in Fig. 3 by nearly 40 kJ mol⁻¹! Therefore, elimination via a 6-membered transition state (Eq. (7)) can be ruled out.



4.4. Charge-remote elimination compared with elimination from neutral ethers

Since the electric charge resides at some distance from the site of elimination, it is not obvious that it should affect the reaction barrier. DFT calculations show that remote protonation has a profound effect. Fig. 4 summarizes the results for neutral **2**, with the dashed curve for *N*-protonated **2** superimposed to illustrate the difference. The endothermicity of *trans*-butene elimination from the neutral ether is

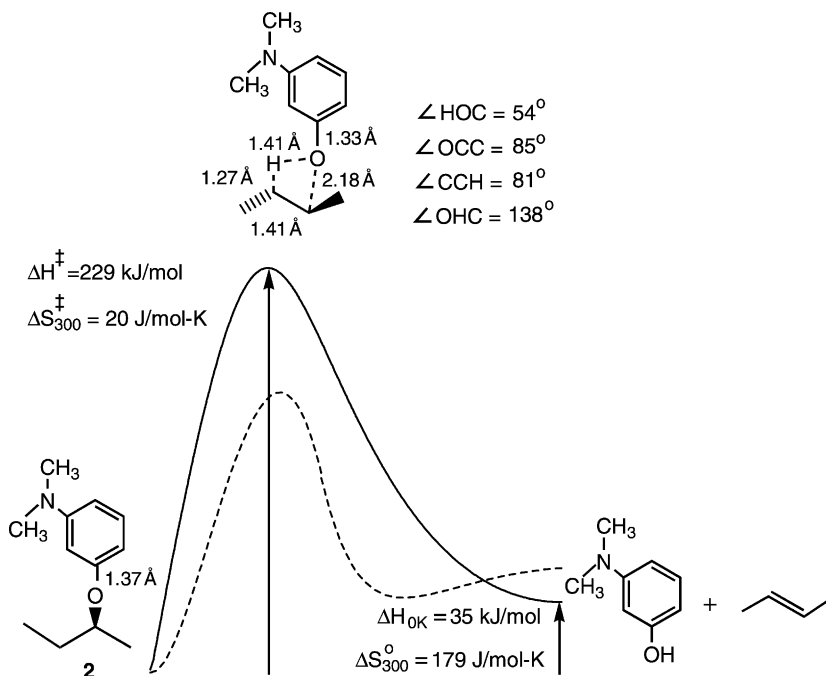


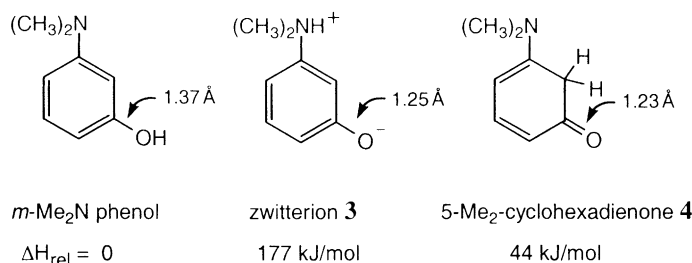
Fig. 4. Schematic DFT energy surface for 4-center elimination of *trans*-2-butene from neutral **2**, with the charge-remote surface (dashed curve) superimposed for comparison. Activation and thermodynamic parameters are listed, as well as relevant geometrical features.

nearly 20 kJ mol^{-1} less than for *N*-protonated **2**, but the barrier height is nearly 45 kJ mol^{-1} higher. The endothermicity difference can be explained by the fact that **2** has a calculated proton affinity 19 kJ mol greater than that of *m*-dimethylaminophenol. The difference in barrier heights requires more detailed interpretation.

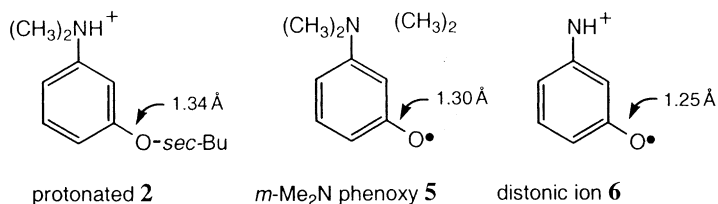
The DFT entropy of activation is less positive for neutral **2** than for *N*-protonated **2**, which implies a tighter transition state. All the atoms in the 4-center transition state in Fig. 4 are coplanar (as in Fig. 3), and

the angles of the quadrilateral do not differ much from those of the transition state for *N*-protonated **2**. Before discussing the atomic distances within this quadrilateral, however, it is worth considering a different set of bond lengths.

The sp^2 C–O bond length in protonated **2** (shown in Scheme 5) calculated to be 0.03 \AA shorter than that of neutral **2**. Consider the C–O bond distances of the fragments in Scheme 4. The C–O bond of zwitterion **3** is 0.12 \AA shorter than that of *m*-dimethylaminophenol, because of the delocalization of the electric charge



Scheme 4.



Scheme 5.

into the benzene ring. Likewise, the calculated C–O bondlengths of *m*-dimethylaminophenoxy radical (shown in Scheme 5) and *m*-dimethylaminophenoxide anion (not shown) are also short, 1.30 and 1.265 Å, respectively. The calculated ring–oxygen C–O bondlengths in neutral **2** and in *m*-dimethylaminophenol are the same within 0.001 Å. That bond shortens by 0.037 Å in the 4-center transition state, a 2.7% shrinkage. In other words, the phenoxy C–O bond becomes shorter in the transition state than in either the reactant or the product. This suggests that the transition state enjoys a contribution from dissociative resonance structures (such as a [5 *sec*-butyl] radical pair or the corresponding ion pair).

This picture is consistent with the Benson–Bose–Haugen model for 4-center transition states, as modified by Maltman and Tschuikow-Roux [12]. That model dissects barrier heights into contributions from four partial bonds plus the dipole–dipole interactions between pairs of these bonds. In a valence-bond interpretation, the model can be described in terms of the participation of the aforementioned dissociative resonance structures. The quantitative model makes use of homolytic bond dissociation energies (BDEs) to estimate the cost of bond lengthening, which corresponds to weighing radical pair resonance structures. Ion-pair dissociative resonance structures are much higher in energy: for neutral **2**, DFT predicts heterolysis of the C–O bond to be >460 kJ mol^{−1} more endothermic than homolysis. In a valence-bond interpretation, the participation of heterolytic dissociative resonance structures represents the role of dipole–dipole interactions.

This change in C–O bondlength is even more pronounced for the charge-remote elimination in Fig. 3,

shortening by 0.042 Å in going from *N*-protonated **2** to the transition state (a 3.1% shrinkage) and then lengthening by 0.048 Å in going to the product ion, *N*-protonated *m*-dimethylaminophenol. The more pronounced shortening of the C–O bondlength in Fig. 3 implies an even greater contribution from dissociative resonance structures in the charge-remote elimination. We advance two reasons for this. First of all, DFT predicts that the proton affinity of the *m*-dimethylaminophenoxy radical (**5**), should be greater than that of **2**. Correspondingly, the C–O bondlength of distonic ion **6** is shorter than that of the neutral radical **5**. As a consequence, the homolytic C–O bond dissociation energy of protonated **2** is calculated to be 31 kJ mol^{−1} lower than that of neutral **2**. This should lower the barrier height at the same time as it leads to further shortening of the C–O bond in the 4-center transition state.

Secondly, remote charge–dipole interactions make a much larger energetic contribution in the case of protonated **2** than do the comparatively weak dipole–dipole interactions in the transition state from neutral **2**. In valence-bond terms, the participation of the [3 *sec*-butyl cation] heterolytic dissociative resonance structure becomes substantial. The heterolytic C–O bond dissociation energy of protonated **2** is calculated to be only 140 kJ mol^{−1} higher than the homolytic BDE. The alteration in bondlength suggests that the transition state in Fig. 3 possesses some character that looks like C–O bond heterolysis to a [3 *sec*-butyl cation] heterolytic resonance structure as well as the expected contribution from a [6 *sec*-butyl radical] homolytic resonance structure.

Other bondlengths also show significant differences between the two transition states. The itinerant

hydrogen from neutral **2** has a longer C–H distance and a shorter O–H distance, which could be taken to suggest that atom transfer has gone further along the reaction coordinate in the neutral than in the charge-remote transition state. However, the breaking C–O bond is shorter in the transition state for neutral **2**, suggesting that its bond cleavage has not gone as far. That is to say, the dimensions of the quadrilateral do not by themselves suggest that one transition state has advanced more along the reaction coordinate than the other.

Instead, the alterations in bond distances are consistent with an increased contribution of the dissociative resonance structures in the charge-remote elimination relative to the neutral. If this notion is extrapolated qualitatively, it predicts that species for which dissociative structures have even lower energies should have progressively lower barriers to alkene expulsion. Such is the case for radical cations: $[R^+ \text{PhO}^\bullet]$ complexes lie lower (relative to the $\text{ROPh}^{\bullet+}$ parent ion) than do the dissociative structures from even-electron precursors. Therefore, the barrier to 4-center elimination is much lower for $\text{ROPh}^{\bullet+}$ than for a charge-remote elimination [3].

4.5. Stereoselective elimination

Despite the differences in activation barriers for radical cation vs. charge-remote elimination, the stereoselectivities are nearly the same. As in the radical cations from phenyl ethers, the difference between the monodeuterated *sec*-butyl diastereomers (*e*-2- β - d_1 and *t*-2- β - d_1) is subtle, while the difference in fragment ion ratios between the 3-hexyl diastereomers (*e*-1- β - d_1 and *t*-1- β - d_1) is much more pronounced. The ratio of *m/z* 138:*m/z* 139 intensity ratios between *e*- and *t*-1- β - d_1 is equal to $r = 2.2$, the same as the ratio of $\text{PhOH}^{\bullet+}:\text{PhOD}^{\bullet+}$ intensity ratios in the SORI-CAD of the corresponding radical cations from the 3-phenoxyhexane-4- d_1 diastereomers [6]. While the *m/z* 123:*m/z* 124 intensity ratios from *e*- and *t*-1- β - d_1 are not reported here, they, too, show the same ratio of ratios, r , albeit with poorer precision. The value of r in the Q-ToF experiments does not

change significantly as collision energy is increased from nominal 12 to 18 eV, but the precision did not improve substantially as the extent of decomposition increased.

The ion intensity ratios in Fig. 2 clearly do not vary linearly with X , the mole fraction of *threo* in a mixture of diastereomers. With five data points, each calibration curve can be exactly fitted to a quartic polynomial. We have looked at the quality of fit with a smaller number of terms. A quadratic expression fits the GC/ion trap data points with $r > 0.9998$: $0.097X^2 + 0.070X + 0.142$. A cubic term must be added in order to give as good a fit for the LC/Q-ToF data points: $0.118X^3 + 0.024X^2 + 0.060X + 0.162$. The curvature of the LC/Q-ToF data can be interpreted in terms of a lower CAD cross-section for *threo* than for *erythro*, since only a small fraction of the ions decomposed under the collision conditions. The GC/ion trap data displays less curvature, but it is harder to understand (since virtually all of the parent ions were dissociated). It may be that a higher energy is needed to dissociate the *threo* fully. Consequently, the kinetic energies of the fragments may be greater and are less efficiently trapped.

In any event, the calibration curves in Fig. 2 show smaller error bars than in our previous studies [6]. The LC/Q-ToF data exhibit larger *m/z* 138:*m/z* 139 intensity ratios than do the GC/ion trap data, probably because $\text{M}^{\bullet+}$ ions do not contaminate the parent ion beam and because ESI produces only the *N*-protonated MH^+ ions. The measurements on mixtures display sufficient precision that the proportion of diastereomers can be measured within $\pm 5\%$ using this approach. Further improvements in precision can be envisaged, which will render MS/MS capable of routine determination of diastereomer ratios in deuterated compounds.

Acknowledgements

The authors are grateful to Henri Audier, in whose laboratory the GC/ion trap experiments were performed, and to Dr. Sophie Bourcier for communicating her ESI/triple quad results. This research was

supported by the CNRS and by NSF grants CHE-9983610 and CHE0078286.

References

- [1] S.J. Abbott, S.R. Jones, S.A. Weinman, F.M. Bockhoff, F.W. McLafferty, J.R. Knowles, *J. Am. Chem. Soc.* 101 (1979) 4323.
- [2] F.B. Burns, T.H. Morton, *J. Am. Chem. Soc.* 98 (1976) 7308.
- [3] G.H. Weddle, R.C. Dunbar, K. Song, T.H. Morton, *J. Am. Chem. Soc.* 117 (1995) 2573.
- [4] R.W. Kondrat, T.H. Morton, *Org. Mass Spectrom.* 23 (1988) 555.
- [5] J.P. Morizur, M.H. Taphanel, P.S. Mayer, T.H. Morton, *J. Org. Chem.* 65 (2000) 381.
- [6] M.H. Taphanel, J.P. Morizur, D. Leblanc, D. Borchardt, T.H. Morton, *Anal. Chem.* 69 (1997) 4191.
- [7] D.J. McAdoo, T.H. Morton, *Acc. Chem. Res.* 26 (1993) 295.
- [8] J.C. Traeger, A. Luna, J.C. Tortajada, T.H. Morton, *J. Phys. Chem. A* 103 (1999) 2348.
- [9] J. Riley, T. Baer, *J. Am. Soc. Mass Spectrom.* 2 (1991) 464.
- [10] S. Bourcier, personal communication.
- [11] E.P.L. Hunter, S.G. Lias, *J. Phys. Chem. Ref. Data* 27 (1998) 413 (NIST ChemistryWebBook <http://webbook.nist.gov/chemistry/ion-ser.html>).
- [12] K.R. Maltman, E. Tschuikow-Roux, *Int. J. Chem. Kinet.* 7 (1975) 363.